Scientia Iranica, Vol. 4, No. 4, pp 190–196

SCIENTIA
IRANICA

Research Note

Electrostatic Charge on Insulating Dust Grains in a Plasma

M.T. Ahmadian*, M.R. Holms[1] and T.P. Armstrong[1]

In this paper, the electrostatic charge state of small insulating solid dust grains in low density plasma is studied. Instead of the common spherical shape, a more realistic cube shaped grain is used in this model. A negative potential is correlated to low yield grains and a positive potential to high yield grains. The resulting equilibrium grain charge is distributed over the surface such that the corners and edges have the largest charge densities. This charge distribution is consistent with an equipotential surface. Secondary electron emission causes slightly higher potential in corners and edges than the rest of the grain. When secondary electron emission becomes important and the average grain potential is close to zero, various regions of the grain are found to have different potentials. No dependence of the final charge state upon initial charge state is observed. This work is the first to approach the problem of grain charging using a nonspherical insulating grain and three dimensional secondary electron emission properties.

INTRODUCTION

The purpose of this paper is to answer three questions with respect to charging of dust grain.

1. Do spherically symmetric grain results hold for more complex geometries?

All grain charging models used up to now for representing a single grain have assumed a spherically symmetric model [1–3]. These calculations all result in a (-2.5 kT/e) for a grain in a Maxwellian plasma when secondary electron emission (SEE) and photo-emission are not important. However, positive potential is possible when SEE and photo-emission are included in the grain charging model. The findings on cubical grain demonstrate that the assumptions made for spherical models are satisfactory.

2. What is the distribution of charge over the grain surface?

The answer to this question is important for determining internal forces of a grain. To keep dust grains together, it is necessary that the internal forces be weaker than the cohesive forces. Charged grains will have larger outward forces than uncharged grains.

It has been shown that the dusty environment in the Saturnian rings are due to the sudden electrostatic ejection of small grains off larger bodies [4–6]. Irregularly shaped grains have a nonuniform distribution of charge and the cube model presented here also reflects this nonuniformity.

Dust behavior in plasma environment has also been an interesting issue for many researchers.

Selwyn et al. [7] and Carlile et al. [8] have found particle accumulation at the sheath - plasma boundary in rings around and above semiconductor wafers in etching by discharges. Geha et al. [9] have revealed that dust particles are commonly found in positive potential traps in plasma.

In these observations they indicated that particles which have different compositions in different types of discharge using different gas mixtures behave similarly. This suggests that the transport of particles depends greatly on fundamental plasma properties and not on the details of the plasma chemistry or excitation mechanisms. All of these observations are also consistent with the particles being negatively charged.

3. Does the grain charge state vary with time?

Previous models have assumed an equilibrium solution to the final grain charge. This was necessary in order to obtain a closed form for the grain potential.

*. *Corresponding author, Department of Mechanical Engineering, Sharif University of Technology, Tehran, I.R. Iran.*

1. *Department of Physics, University of Kansas, Lawrence, Kansas, USA.*

Time variability is used to explain the electrostatic ejection of particles [10] and may affect the behavior of large clouds of dust if grains are charged at different rates. (Grains of the same charge sign might momentarily become oppositely charged and, therefore, attract each other.)

DESCRIPTION OF THE MODEL

The dust grain is modelled by a cube due to its simplicity and the corners and edges which model the irregular shape of a real grain (Figure 1). Each side is subdivided into 16 square charge collection areas making up a 4 by 4 grid (see Figure 1). The cube is divided into discrete cells so that the calculation of the electric field does not require the solution of an electric potential boundary value problem. These charge collection areas will be referred to as cells from here on. Four of the 16 cells on a face lie adjacent to one edge of the cube. The last 4 cells lie at corners. There are 24 side cells, 48 edge cells and 24 corner cells over the entire cube. The charge of a particle striking a cube is added to the total previous charge of that cell. The charge of particles leaving the cell will be subtracted.

The modelled plasma environment assumes a Maxwellian velocity distribution with options of adding a drift velocity towards the grain. The Maxwellian velocity distribution represents the most basic and common plasma conditions modelled for grain charging. The drift velocity will be considered because real grains are not necessarily at rest with respect to the plasma.

Plasma electrons and ions are introduced to the simulation at a boundary with initial position, velocity and species appropriate to the ambient velocity distribution. Figure 2 shows the plasma and cube

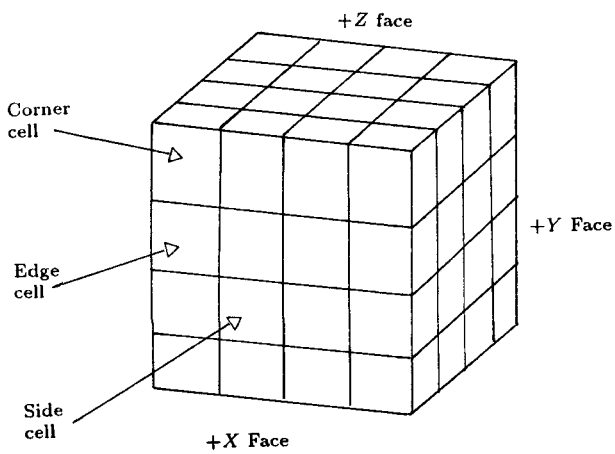

Figure 1. Schematic diagram of grain model and cells.

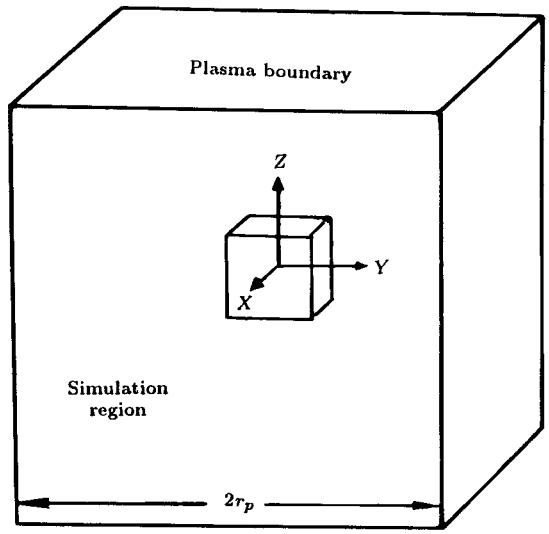

Figure 2. Schematic diagram of coordinate system, grain model and plasma boundary.

boundaries. The shape of the plasma boundary is also cubical with a size chosen large enough so that the electrical fields due to the grain are small yet close enough so that particle trajectories do not take too long to compute.

Once a particle is chosen, its total energy is calculated using the electric potential at the plasma boundary due to the grain charge. If the total energy is less than zero then the particle is not used. Negative energy particles do not exit a collisionless plasma provided that none has left initially.

Electrons or ions introduced at the plasma boundary may either strike the grain or exit through the plasma boundary. Here, it is assumed that a particle that strikes the grain deposits its charge in one of the 96 cells on the surface; furthermore, secondary electrons are produced only if the primary particle is an electron. This is because primary ions at the energies of interest here, produce a negligible number of secondary electrons [11]. Secondary electrons are chosen based on the energy given by the Maxwellian distribution [11]. The emitted secondary electrons have a $\cos\theta$ distribution, where θ is the angle between the surface normal and the secondary electron velocity vector [12]. The emitted secondary electrons may either exit the simulation region or strike the grain model.

Electron or ion trajectories are computed from the plasma boundary to the grain model one at a time using the second order leapfrog method. The electric field, due to the charge distribution on the grain model, controls all particle trajectories and ultimately determines whether an impact will occur for a particle. If a particle impact produces secondary electrons, they are followed simultaneously without interacting with each other until they exit the simulation region. Once this has occurred, a new primary is randomly selected

at the plasma boundary and the above process is repeated.

THE INJECTION OF PARTICLES

The particle injection method consists of four steps. The first of these steps is to determine from which of the 6 sides a particle will enter. Since the electric potential is considered small at the plasma boundary, the flux of plasma particles over a given side is constant. Therefore, a side is chosen randomly depending on the expected relative ambient flux.

The second step is to determine where on the side a particle is to enter. This is easily done by choosing a random number, since the probability of entry is constant everywhere on a given side of the plasma boundary.

The third step is to select a velocity for the particle. Each component of the velocity is given by one of the two following distributions.

$$g_1(v_1) = \gamma_1 v_1 \exp\left(\frac{(v_1 - v_0)^2}{v_{\text{th}}^2}\right) , \quad (1)$$

$$g_2(v_2) = \gamma_2 \exp\left(-\frac{v_2^2}{v_{\text{th}}^2}\right) , \quad (2)$$

where γ_1 and γ_2 are normalization constants. The first distribution is for the component of velocity perpendicular to the plasma boundary and is a Maxwellian distribution weighted by the perpendicular component of velocity v_1. Distribution 2 is for the parallel components of velocity.

The fourth step is to eliminate particles that do not appear to strike the cube. For this purpose, it is assumed that at some radius r_m from the center of the cube the field is dominated by the monopoles moments. All particles that have the closest approach distance equal to r_m have initial kinetic energy and angular momentum that satisfy the following equation:

$$T_p = \frac{1}{2}m\dot{r}_p^2 + \frac{l^2}{2mr_p^2} = kq\left(\frac{1}{r_m} - \frac{1}{r_p}\right) + \frac{l^2}{2mr_p^2} , \quad (3)$$

which assumes conservation of energy and angular momentum. Particles that lie below this parabolic curve in the kinetic energy versus angular momentum plane will pass at some r. If none of these points lie between the curves for $r = r_m$ and $r = r_m - \Delta r$, where r_m is the cube center radius, then r_m has been chosen large enough so that all regions of the kinetic energy versus angular momentum plane, resulting in a cubic impact, are included in particle selection.

PARTICLE MOVER

Particles are moved using the leapfrog method. This method is exactly reversible. The time step is chosen so that results here are insensitive to small change in the length of the time step. Ultimately, this is determined by the cell size on the cube. Speed is very important for this simulation since tens of thousands of particles are typically used per simulation run.

SECONDARY ELECTRON EMISSION

Secondary electrons are introduced into the simulation with velocities chosen randomly from a Maxwellian distribution of temperature T, in a manner similar to that used for primary particles. Equation 2 is used to determine all three components of the secondary velocity. Velocity vector directions are chosen with a $\cos(\theta)$ distribution [12]. The temperature selected for secondaries does not depend on the primary electron or ion temperatures. Secondary electrons enter the simulation region at the primary impact point. The secondary yield is chosen by the following equation:

$$\delta_0(E) = 7.4\delta_M \frac{E}{E_M} \exp\left[-\left(\frac{E}{E_M}\right)^{\frac{1}{2}}\right] ,$$

where $\delta_0(E)$ is the average number of secondary electrons produced per perpendicularly incident primary and E is the primary incident energy. $\delta_0(E)$ has a maximum value of δ_M for primary energy $E = E_m$, determined by experimental fits for typical materials [11]. The angular dependence of the yield is given by:

$$\delta(E,\theta) = \delta_0(E)\exp[2(1 - \cos\theta)] ,$$

where θ is the primary incident angle [13].

Since there can only be an integer number of secondary electrons for a single primary electron, the actual number of secondary electrons produced per impact is given by:

$$N_s = \int (x - s) ,$$

where x is a uniform distribution for random numbers and N_s is the number of secondary electrons produced. The actual distribution for the number of secondary electrons produced per incident primary is not known at present. The distribution described above is the simplest possible and is also consistent with other grain charging models. It should be noted that the average secondary electrons do not carry more energy away than the primary electrons deposit. Once all information is known, the secondaries are followed simultaneously though they do not interact with each other.

SAMPLE RESULTS

The results of one simulation run are presented as a sample of the simulation procedure. This run starts

with a secondary electron yield of 4 and ends with a yield of 6. The transition in yield is not meant to represent any real change in material properties but is a convenient way to observe the change from a negative to a positive net charge. Similar results can be achieved by raising the plasma temperature without changing the secondary electron yield.

The parameters are chosen in a way to simulate a Maxwellian plasma of temperature 1 eV and a grain of size 0.2 microns on an edge. The primary energy at maximum yield is 400 eV and the characteristic temperature of the emitted electron is 0.5 eV.

Figure 3a shows the average charge per cell plotted against the number of trial particles. A trial particle is a particle that is selected at the plasma boundary to be followed regardless of having an impact on the grain. The number of trial particles is proportional to the elapsed time with the scaling factor depending on the plasma density and temperature. The vertical line at 30,000 primaries marks the transition from a secondary electron yield of 4 to a yield of 6. The average charge decreases steadily until the transition in yield occurs at the point where the grain charge snaps to a positive value. The average charge per cell is nearly constant from primary number 40,000 until the end of the simulation at about 87,000 primaries.

Figure 3b shows the average charge per cell for each of the three different types of cells, which are corner, edge, and face cells. These three curves track each other closely as they decrease slowly. At the transition in yield, all three curves become positive and then diverge from each other. The lower curve after the transition corresponds to the average charge per face cell, the middle curve corresponds to the average charge per edge cells and the top curve corresponds to the average charge per corner cell. The corner and edge cell charges approach a constant value while the face cell charge starts to become positive but then returns to a negative value. At about 73,000 primaries, the face cell charge becomes positive. This short transition to positive value is greater than the fluctuations seen on this curve and may indicate a slight instability in the positive corner, positive edge and negative face charge state.

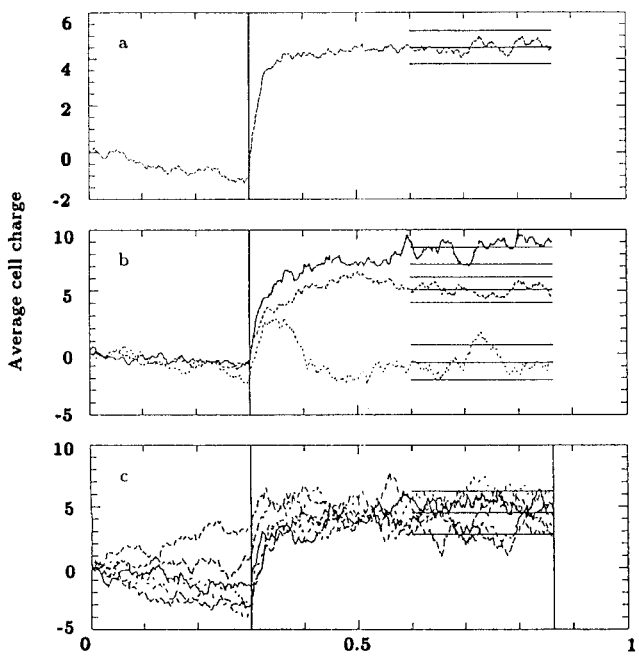

Figure 3. No. of incident primaries ($\times 10^5$).

The distribution of charge among three different types of cells as shown in Figure 3b is consistant with what would be expected. Results from simulation indicate that secondary electron emission is not important and where the grain is negative, essentially the same distribution of charge between the three different types of cells is exhibited except that the face cell charge is of the same sign as the corner and edge cell charges. One possible explanation for this difference is that secondary electrons escape more readily from corner and edge cells than from face cells because of the larger solid angle subtended by the grain close to a face. Secondary electrons emitted from a face cell are more likely to impact the surface of the grain simply because of the grain geometry.

Figure 3b shows the average charge per cell for each of the six sides. Four sides are negative, one side is nearly neutral and the sixth side is positive before the transition in secondary yield. This spread in value of the charge on the different sides is much greater than the largest fluctuations on any single side. This indicates that nonsymmetric grain charge distributions may be stable for grains that have a charge close to zero with respect to higher or lower yield cases. For cases where secondary electron emission is not important, the six sides track fairly close in charge. All six sides are positively charged to approximately the same value after the transition in secondary yield.

In order to estimate an upper limit to the fluctuations in the average charge per cell, it is assumed that the fluctuations for each cell around the average charge per cell are statistically independent of each other. The standard deviation of the cell charge is easily measured for each of the three different types of cells. The fluctuations expected in the average charge per cell taken over all 96 cells is given by σ_A:

$$\sigma_A = (24\sigma_c^2 + 24\sigma_f^2)^{1/2}/96 ,$$

where σ_c, σ_e and σ_f are the standard deviations of the corner, edge and face cell charges taken over all cells over an interval of time. A similar calculation may be made for the fluctuations in the average charge per corner, edge and face cells as well as cells on a given side.

In order to compare σ_A with the actual fluctuations, three horizontal lines were drawn in Figure 3a, extending from about 60,000 primaries to the end of the simulation at 87,000 primaries. If the charge in each of the 96 different cells were uncorrelated, then the fluctuations in this curve would cover all three of these lines. The ratio of the measured standard deviation to σ_A is 0.3. This means that the total grain charge is well constrained while individual cell charges are not. This is to be expected since the monopole moment of the grain charge distribution dominates the higher order moments for large distances from the grain and, therefore, the far away plasma particle motions are controlled by the monopole moment.

A similar procedure is used in Figures 3b and 3c to show the correlation between the cells of a given type (corner, edge or face) and a given side. In Figure 3b, the ratio of the calculated to the measured standard deviation is 0.5, 0.4 and 0.6 for the corner, edge and face cells, respectively. In Figure 3c, this ratio is 1.3. The variation in the distribution of charge between the three different types of cells controls higher ordered moments and, therefore, the lower effect on the surrounding plasma. The ratio in Figure 3c, on the other hand, is greater than that of the average charge per cell on the whole grain. This is especially apparent in Figure 3c before the transition in secondary electron yield. It seems that this independence of the sides from each other is due to the geometry of the problem. Even though dipole moment might dominate the higher moments of the edge and side cells, particles are less likely to be deflected by 90 degrees or more from one side to another. At the same time, the charge fluctuations on one side must offset the fluctuations on other sides for the total grain charge to remain constant. The result demonstrates that the above ratio is greater than one.

Figure 4 shows upper and lower limits for the grain potential. This averaging method is necessary because there is some ambiguity about how to calculate a meaningful potential from the discrete simulation charge distribution. The center of a cell will have a higher potential than a corner of a cell. Therefore, the upper and lower limits are given by the cell center and cell corner potentials, respectively. Before the transition in secondary yield, the grain potential decreases slowly. After the transition, the grain potential is approximately 5 volts.

The parameters for this particular example are chosen in a way that comparison could be made with Mayer-Vernet rain model [3]. Calculation yields a grain potential of about -9 volts for a secondary yield of 4 (before the transition) and a grain potential of +5.8 volts for a secondary yield of 6 (after the transition). The pre-transition potential is not close to -9 volts but it is decreasing up to the transition.

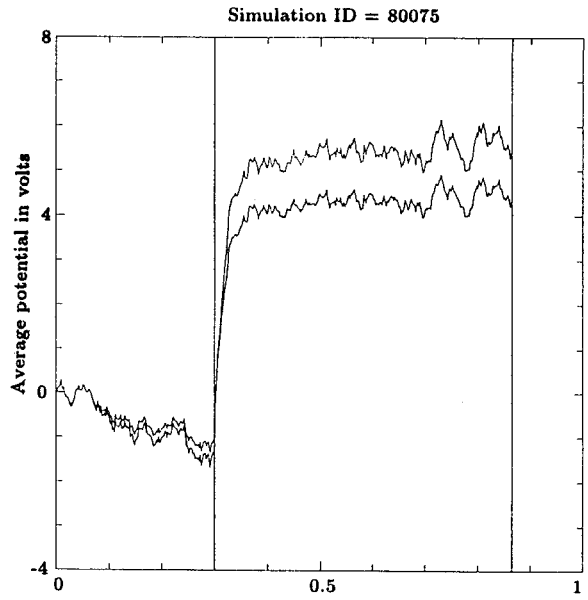

Figure 4. No. of incident primaries ($\times 10^5$).

The post-transition potential is very close to the value predicted by Meyer-Vernet. Since secondary electron emission is modelled differently for this simulation than for Meyer-Vernet calculation, some differences are expected. Meyer-Vernet also predicted triple root situations where a grain could take on three different potentials to neutralize the thermal current, where it was shown that one of these roots is positive, one is negative and one is unstable. In making the transition from negative to positive, it was desirable to find such a situation. However, since the transition results in a change in sign, such a case was not found.

Figure 5 shows potential contours over the surface of the grain at the end of the sample simulation run (about 87,000 primaries). The front three sides are considered (left side or plot) so that the plot is viewed

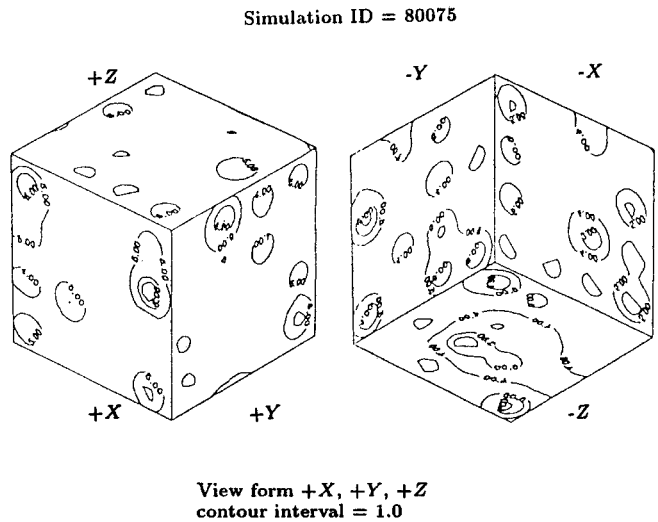

Figure 5. Potential Contours over the surface of the grain cube for simulation run 80075.

Table 1. Summary of the results in this work is preserved.

Result	See Negligible	(Sample Run) See Important		Drift Velocity	
		(Yield=4) $\Phi \leqq 0$	(Yield=6) $\Phi > 0$	$\Phi < 0$	$\Phi > 0$
Comparable with Analytical Results	Yes	Yes	Yes	Yes	Yes
Equipotential Surface	Yes	No Face Cells Slightly Negative	Yes	No	No
Equipotential Sides	Yes	Run too Short	Yes	Yes	Yes
Positive Corners, Negaive Faces	No	Run too Short	Yes	Yes	Yes
Fluctuations in Charge Distribution	No	Run too Short	Maybe Face Cells	No	No
Correlation Between Cell Groupings	Yes	Run too Short	Yes	Yes	Yes

as though the center of the cube. The contours are drawn at 1.0 volt intervals. The 4 by 4 on each side is apparent by the contour rings around the cell centers. These are due to the simulation procedure of representing the cell charge at the cell center and not due to any real physical process. The surface potential is close to 5 volts everywhere with the potential of face cells being slightly lower. This is consistent with Figure 3b which showed a charge distribution consistent with an equipotential grain surface. The negative charge on the face cells has a minimal effect upon the potential there.

The results of this sample simulation run compare well with an analytical model (Meyer-Vernet). In addition, even though the grain is modelled with an insulator, it behaves much like a conducting grain with an equipotential surface. The face cells were of an opposite sign, however, at the resolution available it is hard to say if large gradients in charge density are possible on real grains. The total charge on the grain quickly reached an equilibrium value after the transition in yield in the side cell charge but not enough computer time was available to explore these changes on a larger time scale.

Table 1 gives a summary of the results for three different types of simulation run. The first column, which is labeled "SEE NEGLIGIBLE", corresponds to those simulation runs that have very little or no secondary electron emissions. These compare well with analytical results and generate a grain with an equipotential surface. All runs of this type to date have shown steady state solutions. The correlations between the various cell groupings are similar to those of the sample run above.

These runs are interesting in that they generate a charge distribution that gives equipotential side surfaces with large differences in potential from side to side. The leading sides pick up more positive charges since the ions move slower than the electrons.

CONCLUSIONS

The distribution of charge over the grain surface will result in an equipotential or nearly equipotential surface provided that the plasma environment does not change suddenly. Grains that are positively charged may have negative regions in flat or recessed areas of the grain. Therefore, parts of the grain which may lie in these flat or recessed areas may be electrostatically attracted on a positive grain but repulsed on a negative grain. The size of these regions is not clear from the resolution given by this simulation.

No oscillations in the grain potential were observed on the time scales available with this simulation. It is possible, however, that oscillations occur for small regions of the grain surface. Some signs of an instability in the grain charge distribution were observed that might cause oscillations, giving more time to

slightly different plasma parameters (see discussion of Figure 3b). More computer time will be required to look for grain charge oscillations in detail.

REFERENCES

1. Spitzer, L., *Astrophys. J.*, **93**(369)(1941).
2. Feuerbacher, B., Willis, R.F. and Fitton, B. "Electrostatic potential of interstellargrains", *Astrophy. J.*, **181**, pp 101–113 (1973).
3. Meyer-Vernet, N. "Flip-Flop of electric potential for dust grain in space", *Astron Astrophys*, **105**, pp 98–106 (1983).
4. Hill, J.R. and Mendis, D.A. "The dynamical evolution of the Saturnan ring spokes", *J.Geophys. Res.*, **87**, pp 7413–7420 (1982).
5. Morfill, G.E., Graun, E., Goertz, C.K. and Johnson, T.V. "On the evolution of Saturn's spokes theory", *Icarus*, **53**, pp 230–235 (1983).
6. Goertz, C.K. and Morfill, G. "A model for the formation of spokes in Saturn's ring", *Icarus*, **53**, pp 219–229 (1993).
7. Selwyn, G.S, Singh, J. and Bennett, R.S."In situ laser diagnostic studies of plasma - generated particulate contamination", *J. Vac. Sci. Technol.*, **A7**, pp 2758–2765 (1989).
8. Carlile, R.N., Geha, S., Hanlon, J.F.O and Stewar, J. "Electrostatic trapping of contamination particles in a process plasma environment ", *Appl. Phys. Lett.*, **59**, pp 1167–1169 (1992).
9. Geha, S.G., Carlile, R.N., Hanlon, J.F.O and Selwyn, G.S. "The dependence of contamination particle traps on wafer material and topology," *J. Apple. Phys.*, **72**, pp 374–383 (1992).
10. Meyer-Vernet, N. "Some constraints on particles in Saturn's spoke", *Icarus*, **57**(422) (1984).
11. Sternglass, E.J., *Theory of Secondary Electron Emission under Electron Bombardment*, Science Paper 6-94410-2-p6, Westinghouse Res. Lab., Pittsburgh, Pa (1957).
12. Bunney, R.E., *Secondary Electron Emission*, NASA Grant NaG-570, NASA CR-54366 (1964).
13. Wall, J.A., Burke, A.R. and Fredrickson "Results of literature search on dielectric properties and electron interaction phenomena related to spacecraft charging", *Spacecraft Charging Technology Conference*, Air Force Geophysics Laboratory, AFGL-TR-77-0051 (1977).